ICRF coupling and edge density profile on Tore Supra



2004 Plasma Phys. Control. Fusion 46 1567

(http://iopscience.iop.org/0741-3335/46/10/003)

INSTITUTE OF PHYSICS PUBLISHING PLASMA PHYSICS AND CONTROLLED FUSION

Plasma Phys. Control. Fusion **46** (2004) 1567–1580 PII: S0741-3335(04)81903-1

# ICRF coupling and edge density profile on Tore Supra

**F Clairet[1], L Colas[1], S Heuraux[2] and G Lombard[1]**

[1] Association Euratom-CEA, CEA/DSM/DRFC, Centre de Cadarache, 13108 Saint-Paul-lez-Durance, France
[2] LPMIA, Université Henri Poincaré Nancy I, BP 239, 54506 Vandoeuvre-lès-Nancy, France

Received 8 June 2004
Published 3 September 2004
Online at stacks.iop.org/PPCF/46/1567
doi:10.1088/0741-3335/46/10/003

**Abstract**

In addition to the propagation and absorption of the waves into the plasma, a crucial point in ion cyclotron radiofrequency heating (ICRH) is to know how the energy is coupled to the plasma. The coupling efficiency is experimentally estimated through measurements of the antenna coupling resistance and it is of primary importance to precisely establish its dependence on the plasma parameters. The coupling resistance is highly connected to the density profile, which determines the cut-off positions of the magnetosonic waves for a given radiated wave number spectrum. For a large size tokamak like Tore Supra these cut-off densities range between $10^{18}$ and $10^{19}$ $m^{-3}$, corresponding to the plasma edge. In this study, the RF coupling is investigated with respect to the plasma edge density profile measured by X-mode reflectometry and a characteristic cut-off position of the magnetosonic wave. We show that the edge density is not only a function of the average density but also depends in a complex way, on various edge plasma regimes, the power deposition, or the kind of limiter materials or divertor perturbation used to control the edge. Over a large variety of plasma edge regimes, it is shown how the distance between a characteristic ICRH cut-off density layer and the antenna is the relevant parameter to address the problem of the RF coupling efficiency. Simulation of the coupling process with the three-dimensional antenna code Ion Cyclotron ANTenna compares well with RF measurements, provided that the experimental density profiles are used in the computations.

## 1. Introduction

To reach fusion reactor conditions, plasma scenarios require a large amount of additional power and the use of waves in the ion cyclotron range of frequency is one possibility. On Tore Supra (TS), the ion cyclotron resonance heating (ICRH) [1] system has the larger power coupling capability. It can operate in high-density plasmas and contributes to generate a significant fraction of bootstrap current. However, there is a challenging effort to improve the coupling capabilities of the ICRH power that depends on the edge parameters [2] and especially the

  

edge density. Because the wavenumber spectrum of the ion cyclotron resonance frequency (ICRF) antenna is mostly in the range where vacuum propagation is impossible, the ICRF fast magnetosonic wave (FW) does not propagate below a given cut-off density. Between the cut-off density and the antenna, the wave is evanescent but the evanescent zone is shorter than the perpendicular wavelength so that part of the wave tunnels through it [3]. The FW cut-off, located in the outer part of the plasma, is not only a function of the generator frequency ($\omega_0$) and the cyclotron frequency of ionic species (i) in front the antenna ($\Omega_{ci}$), but also depends on the launched parallel wave number ($k_\parallel$) whose spectrum is mainly governed by antenna geometry. In a simplified case for a plane wave and one ion species, the FW cut-off density can be defined by

$$n_e^{\text{cut-off}}(k_\parallel) \approx \frac{A_i}{Z_i}\left[\frac{\Omega_{ci}}{\omega_0}\left(\frac{\Omega_{ci}}{\omega_0}+1\right)(k_\parallel^2-k_0^2)\right]. \tag{1}$$

On TS, the ICRH antennae are made of two straps and the $k_\parallel$ spectrum depends on the width of the strap, the toroidal distance and the phasing between them. In this paper, the results presented have been obtained in a hydrogen minority heating scheme with a dipole phasing configuration (the current flowing along the straps are in opposite phase). As a consequence the spectrum exhibits two maxima of the excited RF current at $k_{\parallel\max} = \pm 14\,\text{m}^{-1}$ (obtained from the maximum of the FFT of the current distribution into the strap). The coupling capabilities are closely related to antenna matching, and the quality of the wave injection is characterized by the antenna loading resistance ($R_c$). Thus, the RF power ($P_{ICRH}$) launched from the antenna to the plasma is proportional to the coupling resistance, the squared RF current density ($I$) feeding the straps and the strap length. The proportionality factor is the coupling resistance $R_c$:

$$P_{ICRH} = \tfrac{1}{2} R_c I^2 L_{strap}.$$

Due to the broad $k$ spectrum radiated by the antenna, the RF cut-offs take place in a wide plasma edge region. However, we consider in this paper that the main contribution to the RF coupling resistance occurs predominantly at $k_{\parallel\max}$, so that the cut-off density needs to be evaluated at this wavenumber value. Most experimental results presented in this paper were obtained at a moderate magnetic field of 3 T and a ICRH frequency of 48 MHz and a few at nominal field of 3.8 T at 57 MHz have been achieved. In both cases, the corresponding RF cut-off rounds about $1 \times 10^{19}\,\text{m}^{-3}$. However, experimental dependence of the coupling resistance of the ICRH antenna suffers generally from the lack of plasma edge data and is thus plotted assuming a density decay length into the scrape-off layer (SOL) [4] or relatively to the last closed flux surface (LCFS) distance [5] or even versus global plasma parameters (average density, edge safety factor, ...) [6] taking advantage of being experimentally adjustable (so-called engineering plasma parameters) during real time plasma operations. But a detailed analysis of the coupling between the plasma and the antenna requires a local knowledge of the behaviour of the plasma waves near the edge. On TS, fast sweep X-mode reflectometry measures density profiles at the edge with a high radial resolution and offers the opportunity to clearly observe any local changes in the near antenna surroundings. This work accounts then for the experimental evidence of the relationship between the RF coupling resistance and the FW cut-off position. After a brief description of the ICRH experiment in TS and the plasma diagnostics (reflectometers and the antenna probe set-up) required for measuring the density and antenna coupling resistance, the third section is dedicated to experimental results where we draw a collection of different mechanisms influencing the edge density and their effects on the RF coupling. A comparison between the experimental results and simulation code Ion Cyclotron ANTenna (ICANT) is performed in section 4, where it is shown that the RF coupling can be simply drawn from the peripheral profile density with the help of a robust and relatively simple criterion deduced from the fast magnetosonic wave physics.

## 2. ICRH experiment and density profile measurements

The TS is a large size tokamak (major radius 2.4 m, minor radius = 0.72 m) using superconducting toroidal magnets to sustain near-steady-state conditions. The antennae of the TS ICRH system are composed of three RF launchers designed as two-strap antennae. Power delivering capability is 4 MW for each set-up with a current availability of about 30 s. They are located on horizontal ports at the low field side of the torus. Each antenna has actively cooled carbon tiles bumpers on both lateral sides and a Faraday screen with tilted bars coated with $B_4C$ in front of the straps. The distance from the front face bumpers to the straps is 5 cm.

The coupling resistance ($R_c$) is a measure of the power losses in the straps, essentially by wave radiations into the plasma, for 1 A of RF current flowing over a strap of length 1 m. It is calculated from the standing voltage into the antennae measured by 4 probes, one close to either end of each strap, the total transmitted power ($P_{ICRH}$) measured by directional couplers, the impedance of the straps ($Z_0$) and the strap length ($L_{strap}$):

$$P_{ICRH} = \frac{1}{2} R_c \left( \frac{V}{Z_0} \right)^2 L_{strap}.$$

The resistive loss in the antenna has been measured at $0.15\,\Omega\,m^{-1}$. The experimental variations of the coupling resistance occur mainly because of the edge plasma turbulence and an uncertainty of about $\pm 0.5\,\Omega\,m^{-1}$ is estimated.

The edge electron density profiles are measured using a high performance reflectometry combining ultra-fast probing capabilities with high sensitive detection [7]. X-mode polarization is used to provide profile measurements starting from zero density. Experimental variations of $\pm 1$ cm in the profile determination arise mainly from the density fluctuations (micro-turbulence, sawtooth, MHD, etc). The initialization of the profiles is done automatically from the detection of the reflected signal amplitude rise at the initial X-mode cut-off frequency. The uncertainty upon their initial radial positions is approximately $\pm 1$ cm and is due to the fluctuations of this amplitude of the reflected signal. A first set of data was achieved in 1999 with a former 50–75 GHz reflectometer at moderate magnetic field (3 T) providing profiles up to $1.2 \times 10^{19}\,m^{-3}$. Since 2001, profile measurements up to $3 \times 10^{19}\,m^{-3}$ at a high field (3.8 T) have been provided with an additional 75–110 GHz set-up. The reflectometry operates routinely and density profiles are readily available into the TS database for systematic analysis. The reflectometer is located beside the ICRH antenna, unlike in work done previously [8] the density is not measured in front of the antenna.

## 3. Experimental results

On tokamaks, the edge density strongly depends upon the filling gas (He or $D_2$) and, until the end of 1999 TS had been operated with an ergodic divertor (ED) [9] that creates a magnetic perturbation at the plasma periphery thanks to its multipolar coil shape and modifies the boundary conditions. It has been shown how the ED configuration increases the recycling of the particles at the edge and decreases the temperature. It is first necessary to stress how the edge density is modified as a function of the different density regimes occurring on TS. For $D_2$ plasmas, three density regimes (low recycling, high recycling and detachment) were commonly observed with Langmuir probes located inside the ED modules during the ED configuration (while detachment regime was never reached for He plasmas) [10].

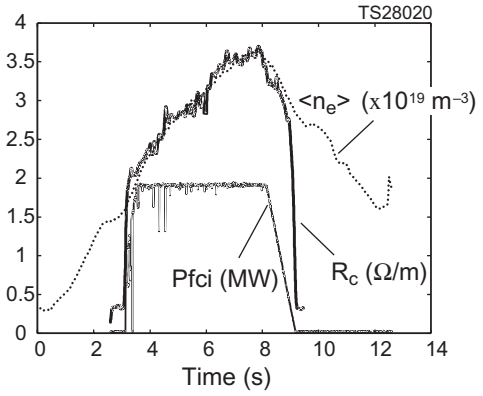


**Figure 1.** Density ramping during ICRH additional power. The coupling resistance increases along with the average plasma density.

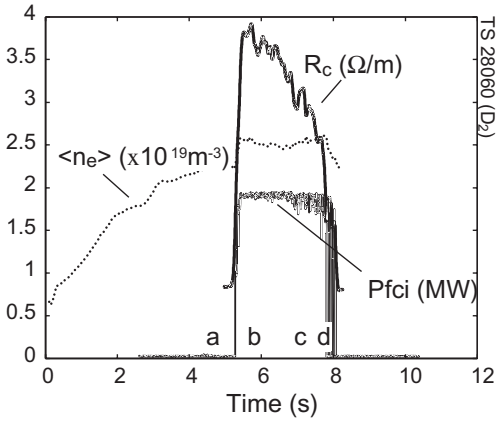


**Figure 2.** Effect of RF heating on the plasma boundary on a $D_2$ plasma. The increase edge density induced by the additional heating drives the plasma to detachment conditions. The RF power couples to the plasma with difficulty until the coupling resistance decreases below the threshold ($R_c \sim 2\,\Omega\,m^{-1}$) where the additional heating is switched off.

### *3.1. Density ramping and plasma detachment*

A first illustration of the effect of the density on the RF coupling is exhibited with a He plasma discharge where a ramp-up of the average density is performed from the low to high recycling regime (figure 1). As the density increases, the RF coupling improves. A simple, linear relationship between the average plasma density and the coupling efficiency can then be drawn, considering that the edge density follows the same behaviour. However, the transition towards the detachment limit for $D_2$ plasma is a particularly good illustration of the local effect of the plasma edge on the RF coupling and the influence of the strap/cut-off distance ($d_{sco}$) on the coupling resistance. It is of particular interest to highlight the plasma detachment as well as the effects of the heating on the plasma boundary. In general, the RF heating induces power deposition at the edge that generally induces a density rise in the SOL. As a consequence the plasma evolves naturally towards high recycling regimes that can even reach the detachment limit as shown in figure 2. In this example, as soon as the RF power is

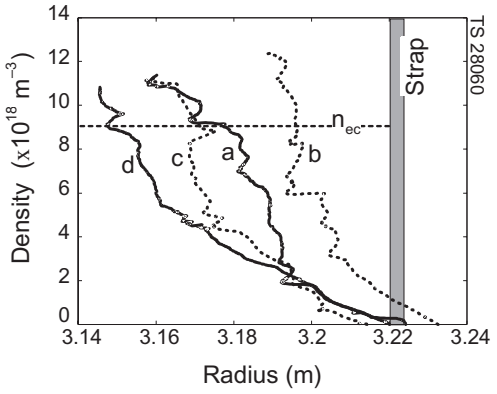


**Figure 3.** Density profile evolution during the discharge referred in figure 2: before ICRH heating phase (a), right after RF power is switched on (b), and with increasing plasma detachment from (c) to (d).

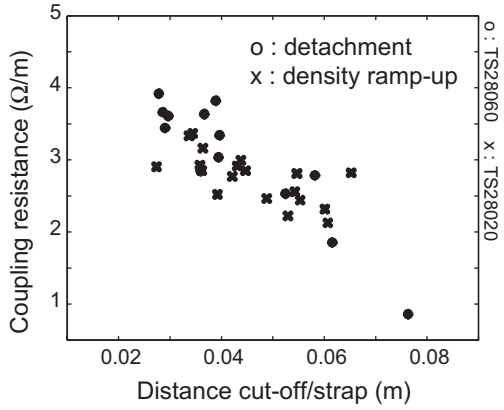


**Figure 4.** Dependence on the distance between the antenna strap and the RF cut-off density layer for the ICRF coupling between the ramp up experiment of figure 1 and the detachment example given in figure 2.

turned on, the average density increases and the coupling is rapidly degraded. In this case, the additional power triggers a plasma detachment. The edge density measurement is performed by the reflectometer during the heating phase (figure 3) and clearly shows that after a sudden increase right after the RF power is turned on, a density collapse occurs constantly so that the distance between the antenna and the fast wave cut-off increases. The coupling resistance then decreases to values ($\sim 2\,\Omega\,\mathrm{m}^{-1}$) where antenna matching is lost and the additional power is turned off.

Each point plotted in figure 4 has been determined from one density profile (no profile averaging is involved) in connection with the corresponding coupling resistance. Comparing the relationship between the coupling resistance and the distance $d_{\mathrm{sco}}$ between both discharges (detachment and ramp-up), we establish that the data overlap shows that this distance can be considered as the critical parameter to account for the RF coupling. We can also observe that no differences of the coupling dependence occur between He and $D_2$ plasmas, as we will show in detail in the next paragraph.

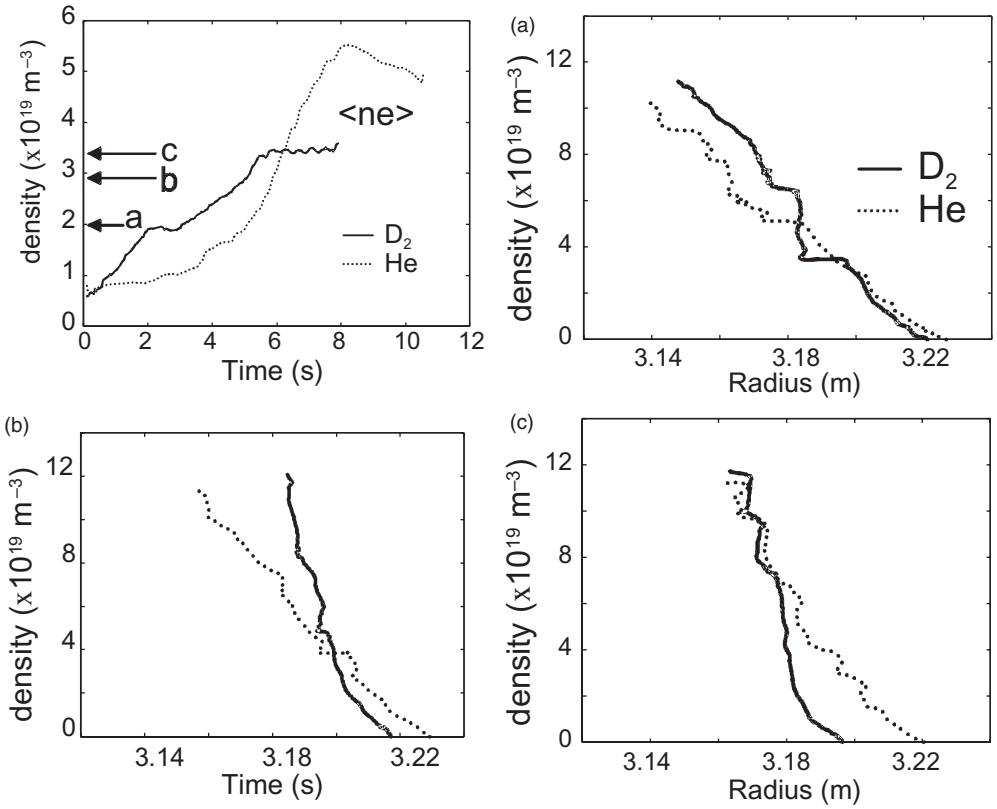


**Figure 5.** Comparison of the edge density profiles between He plasma (· · · · · ·) and $D_2$ plasma (——) during low recycling regime (*a*), high recycling regime (*b*) and detached regime (*c*).

### *3.2. Effect of the gas species: He versus $D_2$*

It is by comparing profiles measured by reflectometry between He and $D_2$ Ohmic plasmas having the same average density and with the same ED perturbation that noticeably different edge behaviours are observed. In figures 5(*a*)–(*c*) a comparison is shown between two discharges (He and $D_2$) with density ramping, where the three regimes are reached in the $D_2$ plasma: during the low recycling regime both $D_2$ and He edge density profiles are comparable but as the density increases, the $D_2$ plasma profile tends to be more peaked than the He profile. When the detachment limit of the $D_2$ plasma occurs, the very edge density collapses while for comparable average density the He plasma edge density profile keeps getting steeper. This result is a key element to account for the better coupling capabilities of $D_2$ plasmas compared to He plasmas [5]. While the coupling properties of the ICRF power do not depend fundamentally on the type of gas used (He or $D_2$), since their mass to charge ratios ($A/Z$), which are involved in the FW cut-off density relationship, are identical, one should expect differences depending on the recycling conditions at the plasma boundary.

We illustrate the role of the edge recycling on the ICRH coupling by comparing (figure 6) similar ED discharges (average density, radius, . . .) with equivalent ($P_{\mathrm{ICRF}} = 1$ MW) additional RF power but containing different gas species (He and $D_2$). The RF coupling is substantially improved (by almost a factor of two) with $D_2$ rather than with He. Global parameters, such as

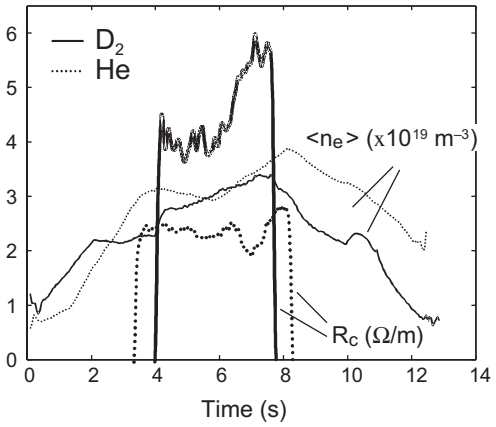


**Figure 6.** For approximately equal average densities, the RF coupling is more efficient for a $D_2$ discharge (a factor of two) compared with He (RF additional power is equal to 1 MW in both cases).

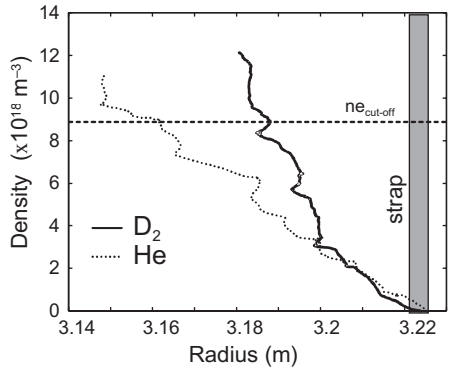


**Figure 7.** Comparison of the edge profiles measured by reflectometry for the two plasma discharges described in figure 6 at $t = 6$ s. For comparable average densities, the edge profile differences account for different boundary density regimes between both gases in such a way that the evanescent region (or distance between the strap and the RF cut-off) is shorter for the $D_2$ discharge rather than for the He discharge.

the average density, are then not relevant to explain such differences in the RF coupling resistance, and an additional edge plasma parameter has to be invoked. Due to the high recycling conditions of both these discharges, strong boundary differences occur and are precisely recorded by the reflectometry system. Measured density profiles (figure 7) exhibit a lower edge density for He rather than for $D_2$ and allow for the direct determination of the distance $d_{\mathrm{sco}}$, between the plasma RF density cut-off and the ICRH strap antenna. This distance is measured to be greater for the He discharge rather than the $D_2$ discharge, so that the ICRH wave evanescent region is increased. Thus, higher RF current is necessary in the straps to couple the same RF power to the plasma. The influence of the fast wave evanescence region is assessed once again (figure 8) through the coupling comparison between both discharges. For $D_2$, as for He, the RF coupling exhibits a close dependence with the $d_{\mathrm{sco}}$ parameter as experimental evidence that this distance operates as a relevant parameter for the coupling efficiency.

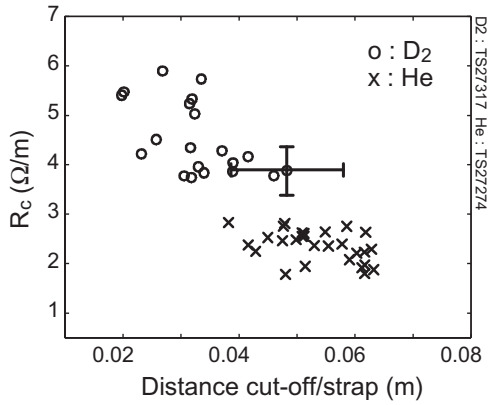


**Figure 8.** ICRH coupling resistance dependence on the distance between the strap and the RF cut-off for the preceding He and $D_2$ discharges. Each point corresponds to one density profile measured by the reflectometer during the additional ICRH power.

### *3.3. Effect of the plasma current*

In the frame of the CIEL project [11], and during the shutdown of the machine in the years 2000–2001, a toroidal pumped limiter (TPL) was installed into the vacuum chamber in order to improve the heat and particle exhaust capabilities by 25 MW in near-steady-state plasma conditions and the ED was removed. In these new conditions the plasmas always lean on the TPL. On tokamaks, particles follow a helical path as they go round the torus. This helical path is determined by the edge safety factor $q_a$, which is the ratio between the toroidal and the poloidal rotations round the torus. Thus, the connection length ($L_c$) between two striking points of a magnetic field line at the LCFS relies on the edge safety factor, $q_a$, through the relation (with $R_0$ major radius): $L_c \sim 2\pi R_0 q_a$. The plasma current influences the poloidal rotation and changes the interaction between the limiter and the plasma boundary. Changing the interaction between the plasma edge and the limiter then modifies the edge density. In addition to the square dependence of the density at the LCFS on the average density usually described in [12], a linear dependence on the edge safety factor (figure 9) was exhibited in TS. However, no clear dependence of the density decay length on the scrape-off was exhibited, to precisely predict the coupling.

The example shown in figure 10 illustrates the influence of the plasma current on the RF coupling through the effect of the edge safety factor on the edge density, and therefore on the distance $d_{sco}$. In this comparison of coupling efficiencies between similar plasma discharges (same antenna position with respect to the LCFS, comparable plasma species ($D_2$), magnetic field (3.8 T) and ICRF frequency (57 MHz)), it appears that the lowest average density discharge leads to a better coupling because of the effect of the connection length that prevails for a highest edge density in agreement with the scaling found in figure 9.

## 4. ICRH coupling resistance calculated with ICANT code

The ICANT code [13] self-consistently calculates the distribution of currents along a set of perfectly conducting surfaces, with which one can model a three-dimensional ICRH antenna. The calculated coupling resistance corresponds to an integration of the coupled modes in the plasma where the major contribution to this integral comes from the vicinity of the maximum

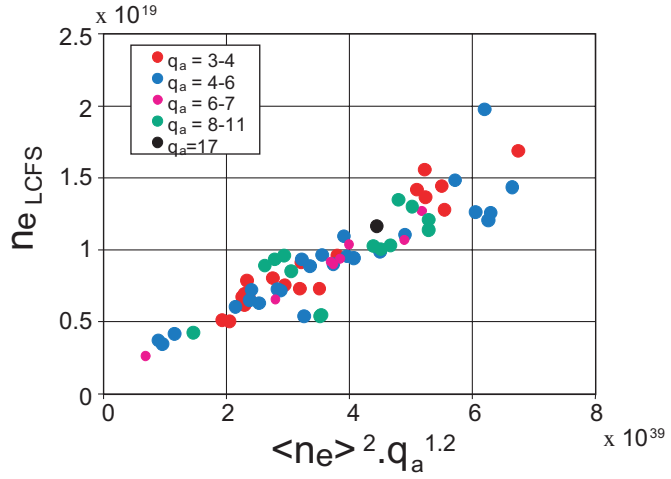


**Figure 9.** Scaling of the density at the LCFS as a function of the safety factor and the average plasma density. These results account for the new LPT configuration of the upgraded TS inner vessel.

(This figure is in colour only in the electronic version)

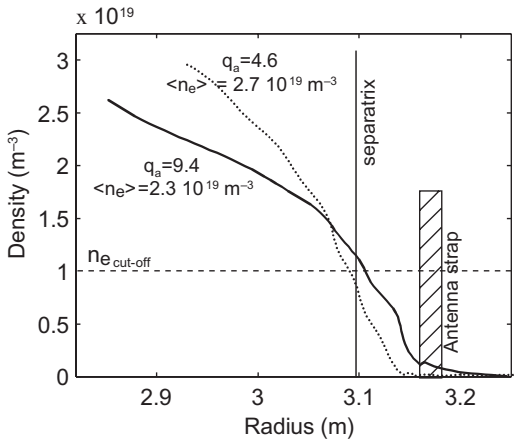


**Figure 10.** These density profiles give an illustration of the influence of the safety factor at low average plasma density onto the edge density according to the scaling in figure 9 and thus the effect on the ICRF coupling resistance. The lowest average density plasma exhibits a better coupling ($R_c = 2.85\,\Omega\,m^{-1}$) than the highest one ($R_c = 2.2\,\Omega\,m^{-1}$) due to a higher edge density and a shorter distance between the strap and the ICRF density cut-off.

of the radiated power spectrum. The expected radial dependence of the coupling should be exponential since

$$R_c \sim \exp\left[-2\int_{\text{strap}}^{x_c(k_z,k_y)} |k_x(x')|\,dx'\right]$$

with $k_x^2 = k_\parallel^2 + k_y^2 - k_0^2$ (see appendix). From this simplified expression we assume that the coupling resistance can be fit by $R_c \sim \exp(-2\langle k_x\rangle * d_{sco})$, where $\langle k_x\rangle$ is a characteristic factor depending on an integration over the radiated spectrum by the antenna. We have to distinguish

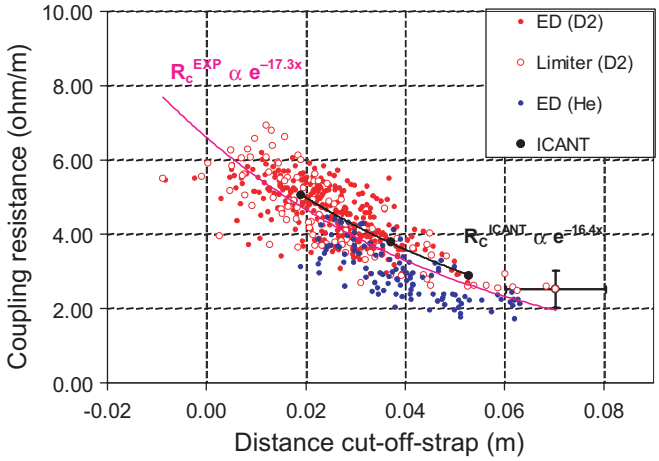


**Figure 11.** Relation between the RF coupling efficiency and the antenna–plasma distance for a collection of 40 discharges performed with a central magnetic field of $B(0) = 3\,\mathrm{T}$ and for an ICRH frequency of $F_{\mathrm{ICRH}} = 48\,\mathrm{MHz}$. Best-fit of the expected exponential decay of the coupling resistance (corrected from the resistive loss of the antennae) brings a maximum wavenumber coupling at $\langle k_x \rangle^{\mathrm{exp}} \sim 8.65\,\mathrm{m}^{-1}$. Experimental results are in close agreement with absolute value ($\langle k_x \rangle^{\mathrm{ICANT}} \sim 8.2\,\mathrm{m}^{-1}$) computed with the ICANT code.

(This figure is in colour only in the electronic version)

this $\langle k_x \rangle$ from the radiated power spectrum in the plasma computed with the ICANT code, which exhibits a maximum parallel wavenumber value around $k_\parallel \sim 9.1\,\mathrm{m}^{-1}$ (different from the strap current spectrum which exhibits a maximum at $k_\parallel \sim 14\,\mathrm{m}^{-1}$).

To compare with the calculations, an experimental database of 40 plasma discharges has been collected. Various experimental conditions (limiter or divertor configuration, He or $D_2$ gas species) involving substantial edge density modifications or different density regimes, have been taken into account to constitute a reasonable statistical description of the antenna–plasma interaction of the ICRH coupling resistance versus the distance between the strap and the cut-off (figure 11). The comparison with the code, where true density profiles are introduced, shows remarkable agreement with the experiment in terms of the absolute value of the coupling resistance as well as the radial dependence. The best-fit experimental radial decay parameter ($\langle k_x \rangle^{\mathrm{exp}} \sim 8.65\,\mathrm{m}^{-1}$) is comparable with the computed one ($\langle k_x \rangle^{\mathrm{ICANT}} \sim 8.2\,\mathrm{m}^{-1}$) determined from the radial dependence of the computed coupling resistance. This comparison between theory and experiment is a good criterion for the code evaluation. $\langle k_x \rangle^{\mathrm{ICANT}}$ is not far from $k_\parallel$ at the maximum of the radiated power spectrum: this is justified by the fact that $k_\parallel^2 > k_y^2 \gg k_0^2$ over the spectrum. In order to compare experimental results with ICANT simulations, knowledge of the density profile in front of the antenna is required. However, since the measurement is made next to the antenna, the profile in the private zone of the antenna is unknown and assumptions are needed to account for the influence of the protection bumpers and of the Faraday screen. A series of simulations (table 1) was performed using the same strap/cut-off distance ($x_{\mathrm{c}}(k_y, k_z)$) parameter in figure 12 for three different vacuum gaps between the plasma and the straps ($x_{\mathrm{i}}$ parameter in figure 12) to mimic the possible profile modification in front of antennae by the bumpers or Faraday screen, thus providing approximate error bars on the ICANT outputs. Table 1 points out the sensitivity of the calculations to boundary plasma conditions and the necessity for good edge profile measurements as well as the difficulty to extrapolate for fusion devices whose edge conditions are unknown.

**Table 1.** Sensitivity of the radial decay wavenumber from the RF coupling spectrum calculated with ICANT simulations and using reflectometry profile with three different vacuum regions between the straps at $R_{\text{strap}} = 3.145\,\text{m}$ and the plasma edge ($R_{\text{edge}}$) (defined as $x_{\text{i}} = 3.155 - R_{\text{edge}}$ in figure 12).

| $x_{\text{i}}$ | 0.025 m | 0.035 m | 0.040 m |
|---|---|---|---|
| $\langle k_x \rangle^{\text{ICANT}}$ | $9.31\,\text{m}^{-1}$ | $8.23\,\text{m}^{-1}$ | $7.68\,\text{m}^{-1}$ |

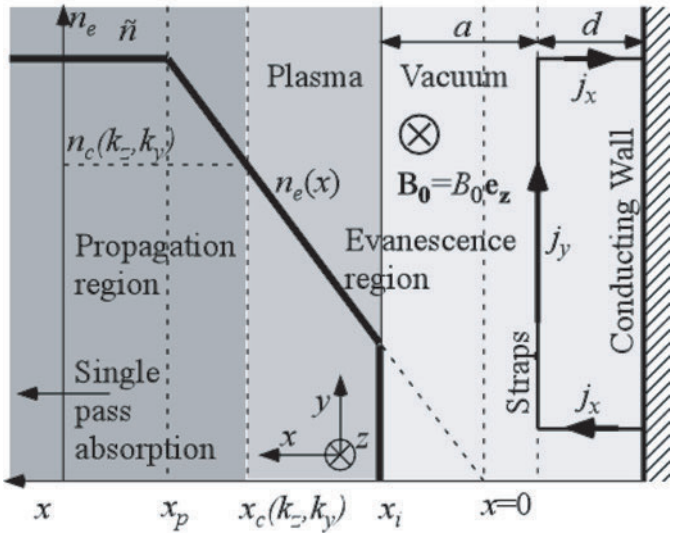


**Figure 12.** Summary of the conventions, assumptions and notations used in power coupling using the ICANT calculation.

## 5. Conclusion

The edge plasma interaction with the ICRH heating system in TS has been studied in relation to various plasma boundary conditions. It has been shown how the density at the edge is governed not only by a global plasma parameter, like the average density, but more surely by local physical processes such as particle recycling conditions along various density regimes, or the connection length between plasma edge limiting elements that dramatically influence the density in the SOL. Nevertheless, we have been able to characterize the ICRH coupling efficiency of the magnetosonic wave with a simple model relating the RF coupling resistance with the edge density profile measured by X-mode reflectometry: the distance between the RF density cut-off and the antenna strap clearly appears to be the relevant parameter experimentally. The wave exponential evanescent model determines, in a first approximation, a RF cut-off density from the maximum of the parallel wavenumber spectrum given by the geometry of the antenna and the distance between the strap and this density in the plasma. This model does not account for any influence of the density gradient effect, being considered of secondary order and probably barely observable experimentally, and does not account for the $k_\parallel$ spectrum width of the antenna. The good agreement found with the numerical code ICANT makes this study particularly relevant for predictions. However, it is pointed out that the use of such simulations for detailed predictions of antenna behaviour can be made only as long as edge density profiles are precisely known.

## Appendix. Coupling resistance dependence on the strap to ICRH cut-off distance

The purpose of this section is to relate the coupled ICRF power to the behaviour of the fast magnetosonic wave between the antenna straps and its peripheral cut-off layer, within some simplifying, yet realistic assumptions, and justify the choice to fit the experimental coupling resistances with an exponential function of the distance between the strap and the characteristic cut-off layer.

To evaluate the ICRH coupling, Maxwell's equations in vacuum are solved in a peripheral slab between a plasma-filled inner region and the vacuum vessel wall. The notations and conventions used are recalled in figure 12 (see also [15]). The ICRF antenna consists of a poloidal current sheet $j_y(y, z)$, located at a radial distance $a$ from the plasma. The antenna connectors are simulated by radial currents $j_x(y, z)$ flowing between these straps and the outer wall, separated by a distance $d$. The RF excitation currents are decomposed into Fourier components in the poloidal ($y$) and toroidal ($z$) directions, with $j_x(k_y, k_z)$ and $j_y(k_y, k_z)$ assumed to be in phase quadrature, consistently with the geometrical symmetries of the TS antennae. Metallic boundary conditions are applied at the outer wall, while the presence of a plasma absorbing the wave is accounted for by a surface impedance matrix $\boldsymbol{\xi}(k_z, k_y)$ at the plasma-vacuum interface. The boundary conditions there, thus, take the form:

$$\frac{E_y(k_z, k_y)}{\omega_0 B_z(k_z, k_y)} = \xi_{11}(k_z, k_y); \qquad E_z = 0; \quad B_y = 0.$$

With these assumptions, and for wavenumbers such that $k_y^2 + k_z^2 > k_0^2$, the real part of the radiated power spectrum can be written as follows [15]:

$$P_r(k_y, k_z) = \mu_0\omega_0 \left| j_y(k_y, k_z) - i j_x(k_y, k_z)\frac{k_y}{p^2}\right|^2 \times \cdots$$
$$\times \left\{ [k_x'(1 - \exp(-2pd))^2 \exp(-2pa)] \left[ k_x'^2 \left[ (1 - \exp(-2p(a+d))) \right.\right.\right.$$
$$\left.\left.\left. - \frac{H^2}{pk_x''}(1 + \exp(-2p(a+d))) \right]^2 + \frac{H^4}{p^2}(1 + \exp(-2p(a+d)))^2 \right]^{-1} \right\}$$

with

$$\xi_{11}(k_y, k_z) = \left[ \frac{1}{k_x'} + \mathrm{i}\frac{1}{k_x''} \right], \qquad H^2 = |k_z^2 - k_0^2|, \qquad p^2 = k_y^2 + k_z^2 - k_0^2.$$

This formula already shows linear dependence of the RF coupling on generator frequency $\omega_0$, for a given value of $\xi_{11}$. It also exhibits a factor $\exp(-2pa)$, due to the evanescence of the ICRF wave in the vacuum gap between the strap and the plasma-filled region. To evaluate the effect of the plasma further within the torus, one must estimate the surface impedance $\xi_{11}(k_z, k_y)$. In the plasma $B_z(k_z, k_y)$ can be deduced from $E_y(k_z, k_y)$ through the propagation relation [14]:

$$\mathrm{i}\left(1 - \frac{n_y^2}{u}\right)\omega_0 B_z = \frac{\mathrm{d}E_y}{\mathrm{d}x} - \mu k_y E_y$$

with

$$u = \varepsilon_{xx} - n_z^2, \qquad \mu = \frac{\varepsilon_{xy}}{u}$$

and

$$\varepsilon_{xx} = 1 + \sum_{j=i,e} \frac{\omega_{pj}^2}{\omega_0^2 - \Omega_{\mathrm{c}j}^2}, \qquad \varepsilon_{xy} = \sum_{j=i,e} \frac{q_j}{|q_j|}\frac{|\Omega_{\mathrm{c}j}|}{\omega_0}\frac{\omega_{ji}^2}{\omega_0^2 - \Omega_{\mathrm{c}j}^2}.$$

The RF electric field $E_y$ is a solution of the wave equation

$$\frac{\mathrm{d}^2 E_y}{\mathrm{d}x^2} - (N_\perp^2(x) - n_y^2)E_y = 0,$$

where the local squared refractive index is

$$N_\perp^2(x) = \frac{L(x) - n_z^2}{S(x) - n_z^2}[R(x) - n_z^2], \qquad n_z = \frac{k_z}{k_0}$$

and $L$, $R$ and $S$ are the usual Stix notations [16]. To go further, radial profiles have to be specified for the plasma parameters. Following Puri's description in [17], $\boldsymbol{B}_0$ is taken to be constant over the edge region. Density profiles for all species are assumed to be homothetic to the electron density profile, taken to be linear between $x = 0 (n_\mathrm{e} = 0)$ and $x = x_\mathrm{p} (n_\mathrm{e} = \tilde{n})$ and constant for $x > x_\mathrm{p}$. The vacuum–plasma interface is located at some position $x_\mathrm{i}$ in this profile (see figure 12). With this geometry:

$$R(x) = 1 + \frac{x}{x_\mathrm{p}} \sum_{j=\mathrm{i,e}} \frac{\omega_{\mathrm{p}j}^2(x_\mathrm{p})}{\Omega_{\mathrm{c}j}(\omega_0 + \Omega_{\mathrm{c}j})}, \qquad x_\mathrm{i} < x < x_\mathrm{p}.$$

If $\tilde{n}$ is high enough the fast wave is propagating at $x = x_\mathrm{p}$ and shows a cut-off at $x = x_\mathrm{c}(k_y, k_z)$. In what follows we focus on the case $x_\mathrm{p} > x_\mathrm{c}(k_y, k_z) > x_\mathrm{i} > 0$, which applies for most of the wavenumbers contributing to RF coupling in typical TS operation. Following Puri the profile of the squared index is further linearized around the cut-off, i.e. one approximates

$$N_\perp^2(x) \approx \alpha[R(x) - n_z^2]$$

with $\alpha$ constant. In practice $\alpha = 1$ at $x = 0$, $\alpha = 2$ at $x = x_\mathrm{c}$ $(k_y = 0, k_z)$, and does not vary much radially (see [15]). Far from the cut-off position, linearization may not be valid but the solution of the wave equation can be matched to WKB-type expressions. Such a simplification turns the wave equation into an Airy equation for each wave vector: putting $X = K[x_\mathrm{c}(n_z, n_y) - x]$ with $K^3 = k_0^2(\alpha/x_\mathrm{p})[R(x_\mathrm{p}) - 1]$ yields

$$\frac{\mathrm{d}^2 E_y}{\mathrm{d}X^2} - X E_y = 0.$$

Assuming single-pass absorption of the fast wave, the particular solution of interest satisfies radiating boundary conditions as $X \to -\infty$, i.e. $E_y(X) \propto \mathrm{Ai}(X) - \mathrm{i}\,\mathrm{Bi}(X)$. Far away in the evanescence zone for the fast wave $X \gg 1$, and the Airy functions can be replaced with their asymptotic expressions [18] to obtain:

$$\frac{\mathrm{d}E_y}{E_y \mathrm{d}x}(x) = |k_x(x)| \left[ -1 + \mathrm{i} \exp\left[ -2 \int_x^{x_\mathrm{c}(k_z,k_y)} |k_x(x')|\,\mathrm{d}x' \right] \right]$$

with $k_x^2(x) = k_\perp^2(x) - k_y^2$. Substituting in the expression for $B_z(x)$ yields, at the plasma vacuum interface:

$$\xi_{11}(x_\mathrm{i}, k_z, k_y) \approx \frac{|k_x(x_\mathrm{i})|(1 - n_y^2/u)}{(|k_x(x_\mathrm{i})| + \mu k_y)^2} \exp\left[ -2 \int_{x_\mathrm{i}}^{x_\mathrm{c}(k_z,k_y)} |k_x(x')|\,\mathrm{d}x' \right] - \mathrm{i} \frac{1 - n_y^2/u}{|k_x(x_\mathrm{i})| + \mu k_y}.$$

The imaginary part of the surface impedance is the one that would be obtained with a plasma step at $x = x_\mathrm{i}$. The real part of the surface impedance characterizes the coupling conditions to the plasma, and exhibits an exponential factor describing the evanescence of the fast wave between the plasma–vacuum interface and the cut-off layer. In the limit $H^2/pk_x' \ll 1$ the

coupled RF power can be simplified and yields:

$$P_r(k_y,k_z) = \mu_0\omega_0 \left| j_y(k_y,k_z) - ij_x(k_y,k_z)\frac{k_y}{p^2}\right|^2 \frac{|k_x(x)|(1-n_y^2/u)}{(|k_x(x)|+\mu k_y)^2}$$
$$\times \cdots \times \left\{(1-\exp(-2pd))^2 \exp\left[-2\int_{\text{strap}}^{x_c(k_z,k_y)} |k_x(x')|\,\mathrm{d}x'\right]\right\}$$
$$\times \left\{\left[(1-\exp(-2p(a+d))) + \frac{H(1-n_y^2/u)}{|k_x(x)|+\mu k_y}(1+\exp(-2p(a+d)))\right]^2\right\}^{-1}.$$

## References


[1] Kuus H, Agarici G, Beaumont B and Brugnetti R 1988 *Proc. 15th Symp. on Fusion Technology (Utrecht, 1988)*
[2] Noterdaeme J M and Van Oost G 1993 *Plasma Phys. Control. Fusion* **35** 1481
[3] Stix T H 1975 *Nucl. Fusion* **15** 737
[4] Hartmann D A, Mayoral M L, Heikkinen J, Noterdaeme J M, Righi E, Lamalle P and Rimini F 2001 *Radio Frequency Power in Plasma (14th Topical Int. Conf. Oxnard CA) AIP Conf. Proc.* vol 595, p 130
[5] Nguyen F, Grosman A, Basiuk V, Fraboulet D, Beaumont B, Bécoulet A, Ghendrih P, Ladurelle L and Meslin B 2000 *J. Nucl. Mater.* **278** 117
[6] Goniche M, Brémond S and Colas L 2003 *Nucl. Fusion* **43** 92
[7] Clairet F, Bottereau C, Chareau J M, Paume M and Sabot R 2001 *Plasma Phys. Control. Fusion* **43** 429
[8] Hanson G R *et al* 1995 *Rev. Sci. Instrum.* **66** 863
Hanson G R *et al* 1995 *Proc. 11th Topical Conf. on Radio Frequency Power in Plasmas (Palm Springs)* (New York: American Institute of Physics) p 463
[9] Ghendrih P, Grosman A and Capes H 1996 *Plasma Phys. Control. Fusion* **38** 1653
[10] Meslin B *et al* 1997 *24th EPS Conf. on Controlled Fusion and Plasma Physics (Berchtensgaden, Germany, 1997)* vol 21 (A–I), p 194
[11] Lipa M *et al* 1998 *Proc. 17th IEEE/NPSS Symp. on Fusion Engineering (San Diego, CA)* IEEE catalogue number 97CB36131, p 353
[12] Wesson J 1997 *Tokamaks* 2nd edn (New York: Oxford University Press)
[13] Pécoul S, Heuraux S, Koch R and Leclert G 2002 *Comput. Phys. Commun.* **146** 166
[14] Descamps P *et al* 1991 *Plasma Phys. Control. Fusion* **33** 1109
[15] Lapuerta S and Colas L 2001 Effet de l'inclinaison du champ magnétique d'un tokamak sur les propriétés d'une antenne radiofréquence *Report* NTT/PHY-2001.009, private communication
[16] Stix T H 1962 *The Theory of Plasma Waves* (New York: McGraw-Hill) p 10
[17] Puri S 1983 *Phys. Fluids* **26** 164
[18] Abramowitz M and Stegun I 1972 *Handbook of Mathematical Functions* (New York: Dover) Formula 10.4.10, 10.4.59, 10.4.61, 10.4.63, 10.4.66